Microfluidic Approach for the Formation of Internally Porous Polymer Particles by Solvent Extraction

Takaichi Watanabe,[a,b] *Carlos G. Lopez,*[a] *Jack F. Douglas,*[c] *Tsutomu Ono,*[b] *João T. Cabral*[a]*

[a] Department of Chemical Engineering, Imperial College London, London SW7 2AZ, UK

[b] Department of Applied Chemistry, Graduate School of Natural Science and Technology, Okayama University, 3-1-1 Tsushima-Naka, Kita-Ku, Okayama 700-8530, Japan

[c] Materials Science and Engineering Division, National Institute of Standards and Technology, Gaithersburg, Maryland 20899, USA

Abstract

We report the controlled formation of internally porous polyelectrolyte particles with diameters ranging from 10 to 100s μm through selective solvent extraction using microfluidics. Solvent-resistant microdevices, fabricated by frontal photopolymerization, encapsulate binary polymer (P) / solvent (S1) mixtures by a carrier solvent phase (C) to form plugs with well-defined radii and low polydispersity; the suspension is then brought in contact with a selective, extraction solvent (S2), miscible with C and S1 but not P, leading to the extraction of S1 from the droplets. This ensuing phase inversion yields polymer capsules with a smooth surface but highly porous internal structure. Depending on the liquid extraction timescale, this stage can be carried out *in-situ*, within the chip, or *ex-situ*, in an

external S2 bath. Bimodal polymer plugs are achieved using asymmetric inverted T-junctions. For this demonstration, we form sodium polystyrene sulfonate (P) particles using water (S1), hexadecane (C) and methylethylketone (S2). We measure droplet extraction rates as a function of drop size and polymer concentration and propose a simple scaling model to guide particle formation. We find that the extraction time required to form particles from liquid droplets does not depend on the initial polymer concentration but is rather proportional to the initial droplet size. The resulting particle size follows a linear relation with the initial droplet size for all polymer concentrations, allowing for the precise control of particle size. The internal particle porous structure exhibits a polymer density gradient ranging from a dense surface skin towards an essentially hollow core. Average particle porosities between 10% to 50% are achieved by varying initial droplet compositions up to 15 wt % polymer. Such particles have potential applications in functional, optical and coating materials.

Introduction

Polymer microparticles with dimensions in the range of 1 to 100s μm are widely used in applications ranging from coatings, optoelectronics controlled drug release, cosmetics, inks and chemical reagents.[1-3] Various techniques including spray drying[3,4] and suspension polymerization[1,2] are often employed to fabricate polymer microparticles. In spray drying, polymer solution droplets are rapidly evaporated, forming hollow polymer particles. In suspension polymerization, a monomer phase containing a polymerization initiator is emulsified by a continuous aqueous phase containing a suitable surfactant, and then polymerized upon heating. Such approaches are well suited for large-scale synthesis but require multi-step preparation and often result in considerable size polydispersity.

Microfluidic technologies provide new opportunities in controlled production of polymeric microparticles.[5,6] Multiphase flows[7] are generally employed although single-phase[8] particle formation has also been reported. Exceptional size control and narrow size distribution, non-spherical shapes and architectures, as well as particles with internal structure, including porous particles and capsules, can be produced.[9-12]

In addition to tuning particle size, controlling the internal particle structure is important to engineer properties (mechanical, transport/separation, delivery, etc.) for practical applications. Multi-layer encapsulation can be effectively implemented using coaxial microchannels to generate liquid-filled polymer capsules[13] or via interfacial reactions.[14,15] Internally porous polymer microparticles are ubiquitous as medical and pharmaceutical carriers of active agents, with increased loading capacity and controlled release kinetics.[16-19] Porosity can be achieved by incorporating porogens during preparation,[20,21] however, these often require subsequent removal under harsh conditions, which may compromise encapsulation. Hydrogen peroxide has been employed as a porogen in water-in-oil-in-water emulsion-solvent evaporation, generating oxygen bubbles, thereby not requiring removal and preventing leakage.[22] Such approaches require emulsion droplet templating and reactive chemical agents, thus involving somewhat difficult solution handling. Therefore, the development of a versatile process for the production of polymer particles with internal porous structure and controlled size remains highly desirable.

We report a straightforward approach, illustrated in Fig. 1, for the production of internally porous polymer microparticles using a microfluidic emulsification and subsequent droplet solidification by solvent extraction. In simple terms, it is the droplet analog of phase inversion used extensively in membrane science to produce asymmetric integrally skinned

membranes with controlled permeability.[23] We employ thiolene microfluidic devices which, unlike polydimethylsiloxane (PDMS),[24] exhibit broad organic solvent resistance, enabling the use of common organic solvents (including hexadecane) as the continuous phase.[25-29] Prepared plugs consisting of polymer (P) and solvent (S1) are carried by a continuous oil phase (C) into a selective solvent phase (S2), which is miscible with S1 and C but not P. The S2 phase extracts S1 from the droplet, inducing volume shrinkage of the droplet and internal phase separation of P- and S1-rich phases, precipitation of the polymer and finally yields particles with a smooth polymer shell and internal porous structure. Depending on the solvent extraction timescale, the precipitation stage can be carried out *in-situ* (Fig. 1a) or *ex-situ* (Fig. 1b). For this demonstration, we prepare droplets of sodium polystyrene sulfonate (P) and water (S1), suspended in hexadecane as carrier phase (C) and use methylethylketone as the extraction solvent (S2). Microfluidic approaches are well suited to produce mono and multi-modal droplet size distributions, with relatively high throughput, and we implement a break-up cascade[30] to create bimodal polymer droplets and thus particle distributions, which are used to form smooth polymer films or tailor drug delivery profiles. We propose a simple descriptive model for the droplet liquid extraction, which quantifies the mechanism and kinetics of the particle formation, and yields particle sizes and extraction timescales. Further, we demonstrate the control of particle porosity by varying the initial polymer concentration and thus the dope viscosity.

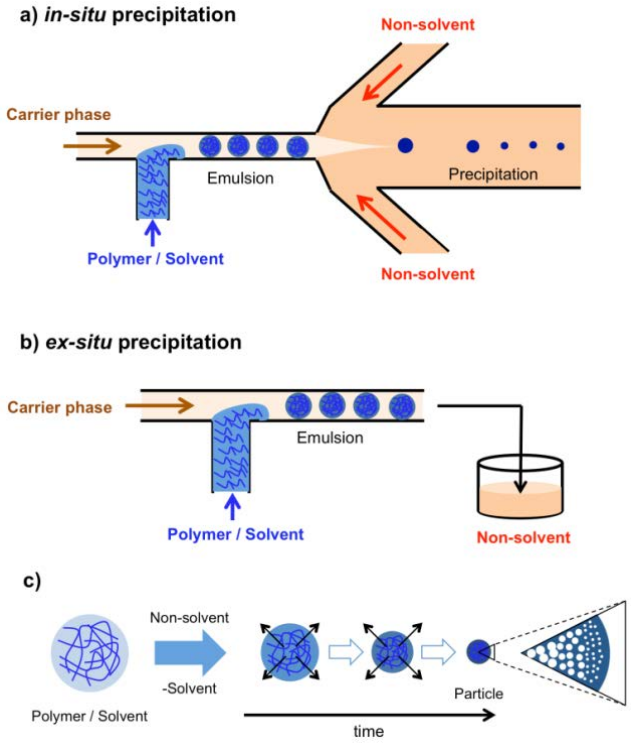

Figure 1. Schematic of NaPSS particle formation via microfluidic emulsification and solvent extraction. (a) *in-situ*, (b) *ex-situ* precipitation approaches, and (c) detail of the polymer solution droplet extraction and precipitation mechanism.

Experimental

Sodium polystyrene sulfonate (NaPSS) with average molecular weight of 70 kg/mol, sorbitan mono-oleate (Span80), *n*-hexadecane (HD), methylethylketone (MEK), ethanol, and acetone were purchased from Sigma-Aldrich and used as received. Microfluidic devices were fabricated by frontal photopolymerization FPP of thiolene optical adhesive (Norland NOA 81) using a procedure reported previously (supplementary info).[25-28] In order to render the channel surfaces hydrophobic, the glass slides were exposed to a 10 wt % of octadecyltrichlorosilane (OTS) / toluene solution for 1 h and dried at 110°C overnight. Inputs were connected to programmable syringe pumps (Braintree Scientific BS-8000) via Teflon tubing. Droplet dispersions were imaged on an inverted optical microscope (Olympus IX71)

equipped with an XY stage (Prior Scientific), CCD camera (Adimec-1000m/D 50fps). A custom-made LabVIEW (National Instruments) programme controls the syringe pumps and XY stage, thresholds images, and analyses drop shapes in real time. The continuous and dispersed phases for all experiments were, respectively, HD containing 0.1 to 3 wt % of Span80, and NaPSS aqueous solutions with concentrations from 0 to 15 wt %. The viscosity of 1 to 40 wt % NaPSS aqueous solutions at 25°C was measured with an Anton Paar stress controlled rheometer (Physica MCR 301) using a cone / plate geometry, with 50 mm diameter and 1° angle; the shear rate was varied between 5 and 500 s^{-1} depending on the sample. Most samples exhibit Newtonian behaviour, with only the highest concentrations exhibiting shear thinning. Polymer concentrations up to 15 wt % PSS, corresponding to viscosities of approximately 1 to 5 mPa s, resulted in stable drop formation. Droplet sizes were varied by changing the flow rate of the continuous phase Q_c , typically within (3.0 to 7.0) mL h^{-1}, while keeping that of the dispersed phase Q_d constant, typically 0.2 mL h^{-1}, corresponding to capillary numbers ($Ca = U\eta/\gamma$, where U is flow velocity, η viscosity and γ interfacial tension) within 0.08 and 0.29. The internal structure of the microparticles was probed by Scanning Electron Microscopy (TM-1000, Hitachi), after 6 h drying and sectioned using a blade or crushed between glass slides.

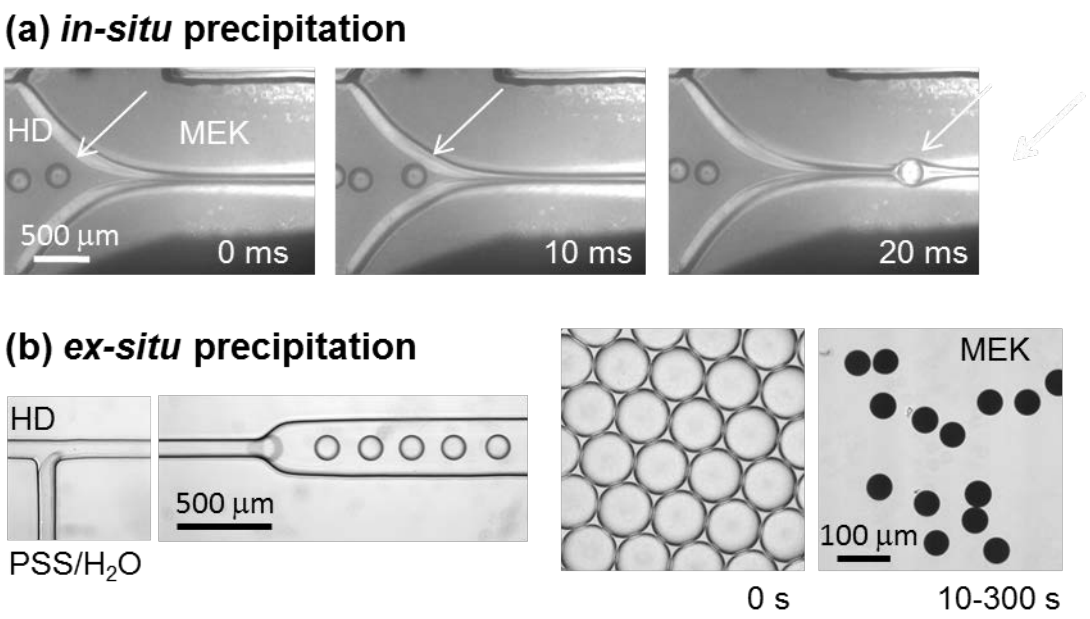

Figure 2. Implementation of (a) *in-situ* and (b) *ex-situ* precipitation approaches. The characteristic timescales of solvent extraction for the current PSS/H_2O/MEK system are better suited for *ex-situ* precipitation, ranging from 10 to 300 s, depending on initial drop size and polymer concentration (bottom right panel shown after 5 min).

Results and Discussion

Two approaches have been demonstrated to produce polymer particles, depicted in Fig. 1 and 2. The first method is an "*in-situ* precipitation" that generates liquid droplets and then induces phase inversion to form particles *within* the microchannel, while the second, "*ex-situ* precipitation", forms and collects droplets within the device, which are then precipitated outside the device. *In-situ* precipitation comprises a T-junction, where polymer solution plugs are formed and suspended in a carrier phase, followed by a flow focusing junction which confines the droplets with converging non-solvent streams. The *ex-situ* approach is simpler and requires only a T-junction to form polymer solution plugs and an outlet stream that is added dropwise to an excess non-solvent bath (5 mL, corresponding to 10 to 100 fold

volume). In both cases, once the polymer solution droplets are brought in contact with the non-solvent MEK phase (S2), water (S1) is extracted from the droplet into the MEK phase due to its higher solubility, thereby causing droplet size reduction, supersaturation of the polymer within the droplets and, eventually, polymer precipitation to form a dispersion of solid porous particles. The extraction process is illustrated Fig. 1c. The kinetics of the extraction and phase inversion inevitably depend on droplet size, polymer solution (or dope) viscosity (and thus molecular weight), mixture thermodynamics and mutual diffusion coefficient. For this system and droplet diameters ranging from 50 to 700 μm, we find that the process typically requires 10 to 300 s. For this system, the timescales associated with solvent extraction are much longer than those of microflow focusing (≈ 10 ms) and microchannel convection of the *in-situ* approach (Fig 2a); such system would require long residence times and large non-solvent consumption. We have therefore opted for the *ex-situ* approach to further investigate this system.

We employed aqueous NaPSS solutions with concentration ranging from 2.5 to 15 wt % as dispersed phase. Figure 3a shows the specific viscosity η_{sp} of aqueous solutions of NaPSS in water as a function of concentration ($\eta_{sp} \equiv (\eta - \eta_{H2O}) / \eta_{H2O}$, where η_{H2O} is the viscosity of water). The lines are scaling predictions derived from the *de Gennes* isotropic model for dilute, semidilute unentangled and concentrated regimes of polyelectrolytes.[31] We estimate the amount of salt to monomer ratio to be of the order of 1:3 to 1:4 present in our commercial system, corresponding to molarities of ≈ 0.03-0.3M depending on initial polymer concentration. Muthukumar and co-workers (0.01 M to 1M) recently reported on the crystallization of NaCl in dilute aqueous NaPSS (0.005-0.5 wt %) droplets of several mm in air;[32] the concentration range of this study corresponds to the top

left panel of their Fig. 1, and our water extraction times are considerably shorter than their evaporation times. We estimate the overlap concentration c^* from the reciprocal of the intrinsic viscosity [η] (obtained from linear extrapolation of the reduced viscosity to zero concentration) to be $c^* \approx 2$ wt%. The crossover to the 'concentrated' regime is observed at around 13 wt % polymer concentration. Above 15 wt % NaPSS, the shear viscosity exceeds $\eta \approx 5$ mPa s, and drop production becomes irregular due to entrainment of the dispersed stream. NaPSS aqueous droplets were produced reliably as illustrated in the inset of Fig. 3b, with diameters tuned by channel geometry and by varying the flow rate of the continuous phase (Q_c) from 3.0 to 7.0 mL h^{-1} while keeping that of the dispersed phase (Q_d) constant at 0.2 mL h^{-1}, yielding $Ca < 1$. Figure 3b shows sequential droplet sizes (200 samples) obtained with a T-junction with 120 μm channel width and 100 μm height. Droplet sizes exhibited relatively narrow size distributions with coefficient of variation (defined as CV(%)= standard deviation / average diameter) below 5.0 %. Size fluctuations are likely caused by small pressure fluctuations (in our volume-driven system) and automated droplet edge thresholding and detection during LabVIEW image analysis. Figure 3 compiles droplet size distributions obtained in Fig. 3b, by adjusting the continuous phase flow rate, for a fixed microchannel geometry, interfacial tension and viscosities; average diameters are provided in Fig 3d. By adjusting microchannel dimensions we readily achieve droplet sizes from 50 μm to more than 700 μm in diameter.

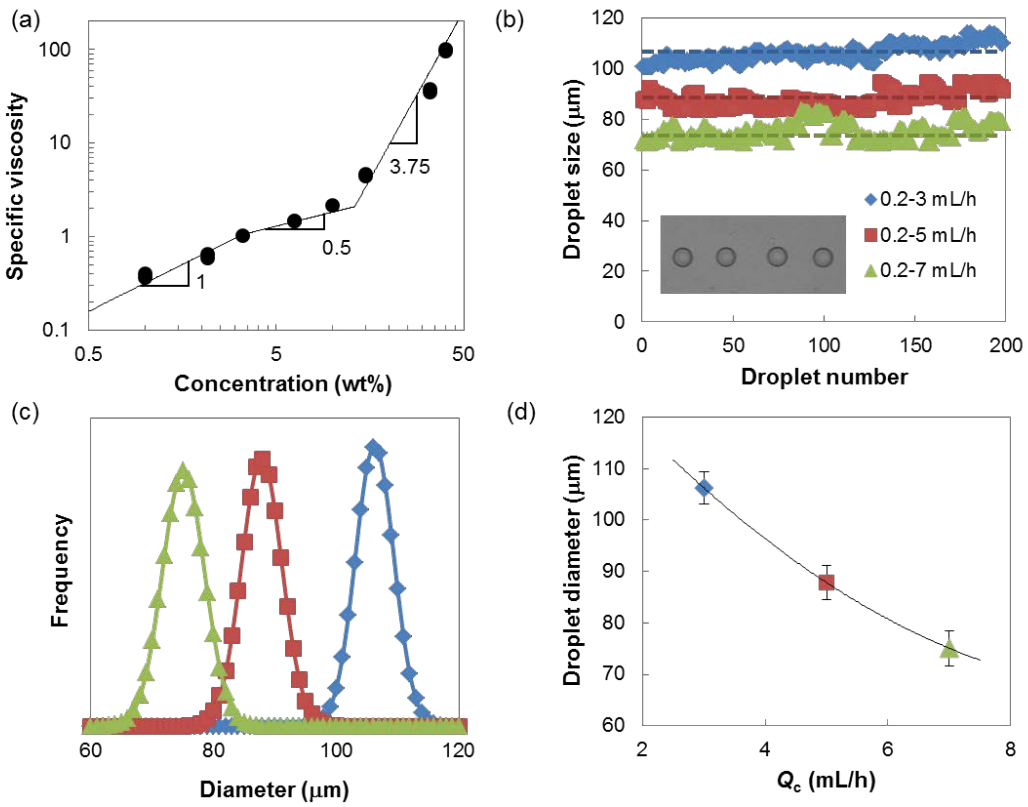

Figure 3. (a) Specific viscosity of aqueous solutions of NaPSS in water as a function of concentration. (b) Initial droplet size control by varying carrier phase flow rate (Q_c = 3 to 7 mL h^{-1}), at fixed polymer concentration (2.5 wt %) and dispersed flow rate (Q_d = 0.2 mL h^{-1}); typical optical micrograph (inset); (c) corresponding droplet size distributions and (d) dependence of average droplet diameter on carrier phase flow rate Q_c; uncertainties are estimated from the standard deviation of approximately 200 droplets.

To demonstrate the controlled generation of plugs with bimodal size distribution, leading to bimodal particles, we employ an inverted asymmetric T-junction geometry, [30] which asymmetrically splits plugs formed upstream. The criterion for breakup at the stagnation point is determined by *Ca* and an initial extension ε_0 defined as the ratio of the initial plug length l_0 to circumference πw_0.[30,33,34] The volume ratio of split droplets is tuned

by the hydrodynamic resistance T-junction outlets, given by $R = 12\eta L/(w_x w_y^3)$, where L is the length of a channel and w_y is the smaller of the two widths (w_x, w_y) of its rectangular cross-section. Figure 4a illustrates a breakup event and Fig. 4b establishes the boundaries between breakup and non-breakup conditions in our system. We deliberately target a small size droplet difference of 20% and Fig. 4c depicts the resulting size distribution computed from optical microscopy, yielding a well-resolved bimodal distribution with each population exhibiting a rather narrow polydispersity (CV < 1.5%). The production of bi- and multi-modal droplet (and thus particle) size distributions is thus readily achieved in our FPP devices by employing inverted asymmetric T-junction cascades. .

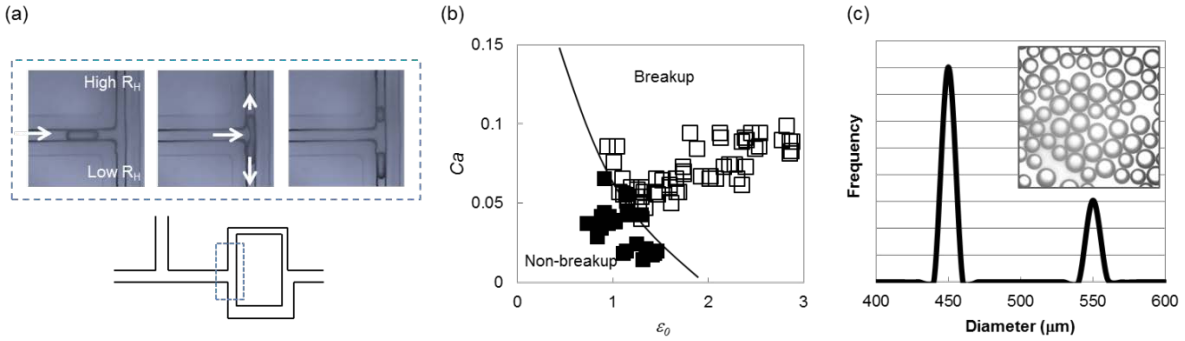

Figure 4. Bimodal plug formation using an inverted T-junction. (a) Optical microscope images of geometry mediated droplet breakup and a schematic illustration of the cascade microfluidic device. (b) Boundary for breakup and non-breakup conditions. (c) Droplet size distribution and corresponding optical micrograph of the emulsion (inset).

Particle formation is triggered by bringing polymer droplets suspended in hexadecane (C) into contact with MEK (S2) to induce water (S1) extraction and polymer particle formation. For the *in-situ* precipitation approach, depicted in Fig 2a, the droplet suspension was focused by two MEK streams at a wider downstream microchannel. The

MEK flow rate was much higher (25 mL h^{-1} each) compared to the other phases (3.1 mL h^{-1} in total). Clear droplet shrinkage and polymer particle formation was not observed within the microchannel, due to the relatively slow extraction of water into MEK compared to convection times (depicted in Fig 2a). Considerably longer (~1000×) channel lengths are required to complete particle formation within the channel. Further, varying initial droplet size and total volumetric flow rates would require adjusting channel length. We have thus concentrated on polymer particle preparation via *ex-situ* precipitation, illustrated in Fig 2b, by introducing droplets directly into a container with pure MEK outside of the microchannel.

Figure 5a shows sequential optical microscope images of a representative polymer droplet in MEK phase, whose size decreases with extraction time. The refractive index contrast between the droplet and the MEK phase first decreases with time (within 0-8 s) and then increases upon solidification. Upon contact between the emulsion and MEK phases, water molecules from within droplets dissolve in the surrounding MEK, given the high solubility (water solubility in MEK is 10 wt % at 20^{o}C), and full MEK/HD miscibility. The NaPSS concentration thereby increases and eventually reaches supersaturation, leading to polymer precipitation. Figure 5b depicts the liquid extraction kinetics of selected 2.5 wt% NaPSS droplets (indicated by different symbols) of radius R = 45 μm as a function of time. After a relatively slow droplet shrinkage stage within 2 s, the radius decreases approximately linearly with time up to 7-10 s; thereafter, the shrinkage slows down and drop dimensions reach constant values in approximately 15-17 s. The initial slow decrease in size is associated with the presence of a small amount of HD surrounding the water droplets, which must first dissolve in the MEK phase, which hinders the initial water extraction. Deceleration of droplet shrinkage in the last stages of droplet extraction is caused by the increase of droplet viscosity

as the polymer concentration increases, while MEK remains in great excess throughout extraction.

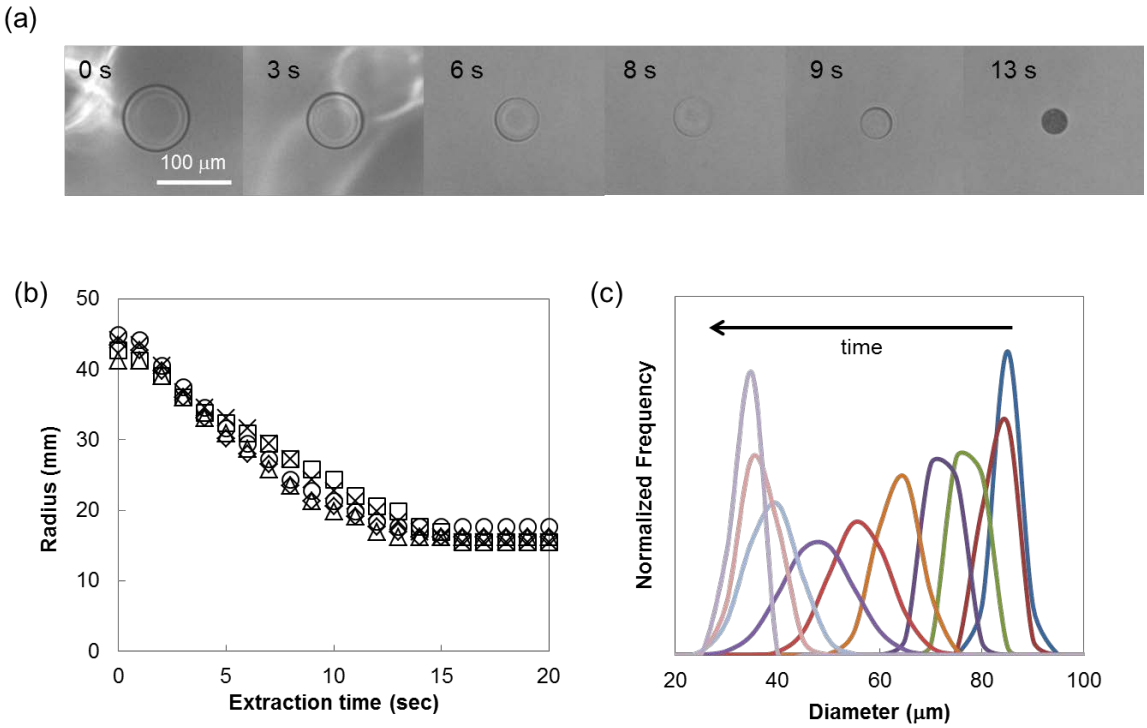

Figure 5. Kinetics of droplet extraction from an initial polymer concentration at 2.5 wt %. (a) Optical microscope image of droplets dispersed in MEK during solvent extraction (b) Average droplet size reduction as a function of extraction time for nominally identical droplets, indicated by symbols; (c) Histogram of droplet size distributions (computed from 10 different droplets) during extraction, over the time scale shown in (b).

Figure 5c follows the size distribution of a representative ensemble of 10 polymer solution droplets during solvent extraction. The initial droplet size distribution, arising from the microfluidic T-junction, is relatively narrow; as the droplet size decreases, the distribution broadens before narrowing again approaching completion. Broadening of the size distribution during solvent extraction is likely due to local concentration differences within the non-solvent bath, due to the initial presence of HD surrounding droplets, as well as droplet

crowding, during extraction. Given the large excess of non-solvent MEK, in which both HD and H_2O are soluble, the final environment is largely pure MEK (≈ 99% by volume). Our results show that the final particle dimensions are not affected by extraction pathway fluctuations as all initial droplet sizes eventually converge towards the same final size. From these results, we conclude that the *ex-situ* approach is suitable not only to produce monodisperse NaPSS microparticles in a continuous manner but also to quantitatively evaluate the solvent extraction process.

We analyzed droplet extraction kinetics under various conditions to further understand the mechanism and kinetics of polymer particle formation. We model the process by first considering the extraction of a water droplet with dissolved polymer in a background medium in which the droplet is soluble. The radius-time relation is rather complex for a droplet of this kind when the moving nature of the droplet is fully taken into account.[35-37] Further, an encapsulating polymer-rich barrier is expected to develop at the droplet interface during solvent extraction, thereby inhibiting interfacial transport. We are therefore dealing with a highly complex transport problem. We propose a simple model that focuses on essential observable properties of droplet solvent extraction. The first passage time of a solvent molecule within the droplet to the droplet boundary is expected to scale as $\tau \sim R^2/D$, where R is the drop size and D the diffusion coefficient, in proportion to the interfacial area, as proposed by the classical Hixson-Crowell theory of solid particle dissolution.[39,40] We then assume that the solvent flux scales in proportion to the solvent diffusion coefficient, $\phi \sim D$, independent of droplet size, and thus extraction occurs at constant flux, as in the dissolution of a solid particle rather than as a fluid droplet.[38] We also define the final particle size, upon completion of the solvent extraction, as the 'terminal radius' R_∞ which is an experimental

observable. The theoretical description of particle formation is complex as it must account for this saturation in particle size at long times, as well as for the diffusive process underlying the solvent extraction and the skin effect.

In fact, the size evolution of a single dissolving liquid drop in another medium is itself a complex moving boundary reaction-diffusion type problem,[35-37] but the moving nature of the boundary can be neglected in the dissolution of large droplets under conditions where the rate of diffusion is limiting the dissolution process.[38] This assumption has recently been validated with liquid (aniline) microdroplets disolving in water.[41] The classical Epstein-Plesset theory of droplet dissolution assumes as a Fickian diffusive process and that the droplet radius changes with time according to $t^{1/2}$. Recent work has also shown that mode coupling effects described by dynamical interfacial tension (Kortweg forces) can also change the dissolution exponent closer to t^{1}, when the dissolving droplet and surrounding solvent are highly miscible and the droplet highly unstable.[42] Further, in our case, inhibited transport is expected due the formation of a polymer layer at the droplet boundary or accumulation of residual surfactant, as droplet extraction proceeds.

It is common in many non-homogeneous materials for the concentration dependence of D, and other factors related to the free energy of mixing, to lead to non-Fickian transport in which interfaces evolve with a power law other than 1/2 (e.g., the coarsening or dissolution of phase separated structures, or homogenization after a change of thermodynamic conditions) and inspection of the numerical solutions to the problem of dissolving droplets shows that size of the drops varies in a generalized power form to a good approximation, although with variable power. Taking the droplet size saturation and the power law evolution of the droplet size with time as basic features of our model, we take the

droplet radius $R(t)$ as a function of time t to be described by the functional form,

$$R(t) = (R_0 - R_\infty)(1 - \frac{t}{\tau})^\alpha + R_\infty \quad (1)$$

where R_0 is the initial droplet radius, R_∞ is the final particle size, and τ is the 'extraction time', i.e. required to reach constant particle radius. We call the parameter α, characterizing the non-Fickian pattern of interfacial movement a 'hyperbolicity' or 'non-Fickian' parameter. This expression for droplet size evolution also incorporates the standard Hixson-Cromwell model of particle dissolution, where we then have a linear particle dissolution kinetics, $R(t) = R_0(1 - t/\tau)$, corresponding to $\alpha = 1$. Variations on the Hixson-Crowell model have been extensive studied in the context of the dissolution of pharmaceutical drugs where a phenomenological α parameter, relating to non-Fickian diffusion, which can notably be greater than 1, corresponding to super-diffusion processes (cf Sect. 2.6 and Table I of Ref [40]) We find that all our droplet extraction kinetic data for variable initial size and polymer concentration are well fitted by this scaling model in eq. (1), with physically significant fitting parameters: τ, R_∞, and α. We discuss our observations in terms of these basic parameters characterizing the kinetics of the extraction process.

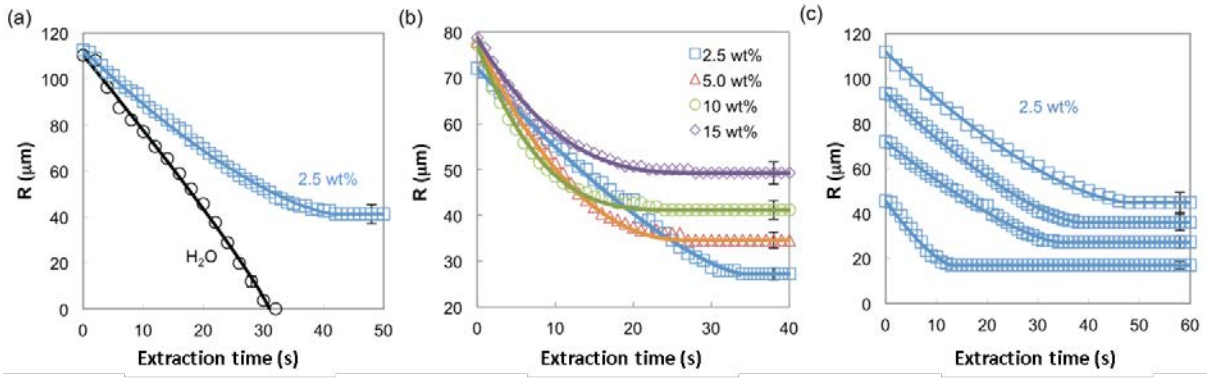

Figure 6. Kinetics of droplet extraction, measured by change in radius (R) as a function of time. (a) Comparison of pure H_2O dissolution (○) and H_2O extraction from NaPSS/ H_2O

(2.5% □) droplets in MEK. (b) Extraction of droplets with similar initial size but varying polymer concentrations, from 2.5 wt % (□) to 15 wt % (◊). (c) Extraction profile for droplets of fixed initial polymer concentration (2.5 wt %) and various initial sizes.

Figure 6a compares the dissolution kinetics of a pure water droplet and the water extraction of an aqueous droplet containing NaPSS at 2.5 wt %, both in MEK. Model fitting yields $\alpha = 0.9$ for pure water and 1.4 for the polymer droplet, consistent across all data at this polymer concentration. Polymer solution droplets exhibit a radius that decreases with time and decelerates as the size approaches a constant value. In contrast, water droplets dissolve fully, decreasing in size until vanishing; specifically R decreases approximately linearly within 20 s (for R_0= 110 μm), beyond which the dissolution rate *increases* gradually until dissolution at τ=31 s. The acceleration is due to an increase of surface-to-volume ratio as the drop shrinks, corresponding to $\alpha < 1$, while polymer solution droplets increase in viscosity before solidification, yielding $\alpha > 1$. Figure 6 (b) compiles extraction kinetics of droplets with similar initial sizes but different polymer concentration. Trivially, the final particle size depends strongly on the initial concentration, and the higher the initial polymer concentration, the larger the particle extracted. The non-Fickian parameter α, describing the curvature of the liquid extraction plots, appears to increase as the initial polymer concentration increases, which implies that the initial shrinking rate increases with increasing of initial polymer concentration. The dependence of extraction time τ on polymer content is less obvious, and requires statistical analysis (presented below), which could be due to the slow dependence of polymer solution viscosity η with concentration, from 2.5 to 15 wt % (Fig 3a). This led us to probe the internal particle structure, shown in Fig 7.

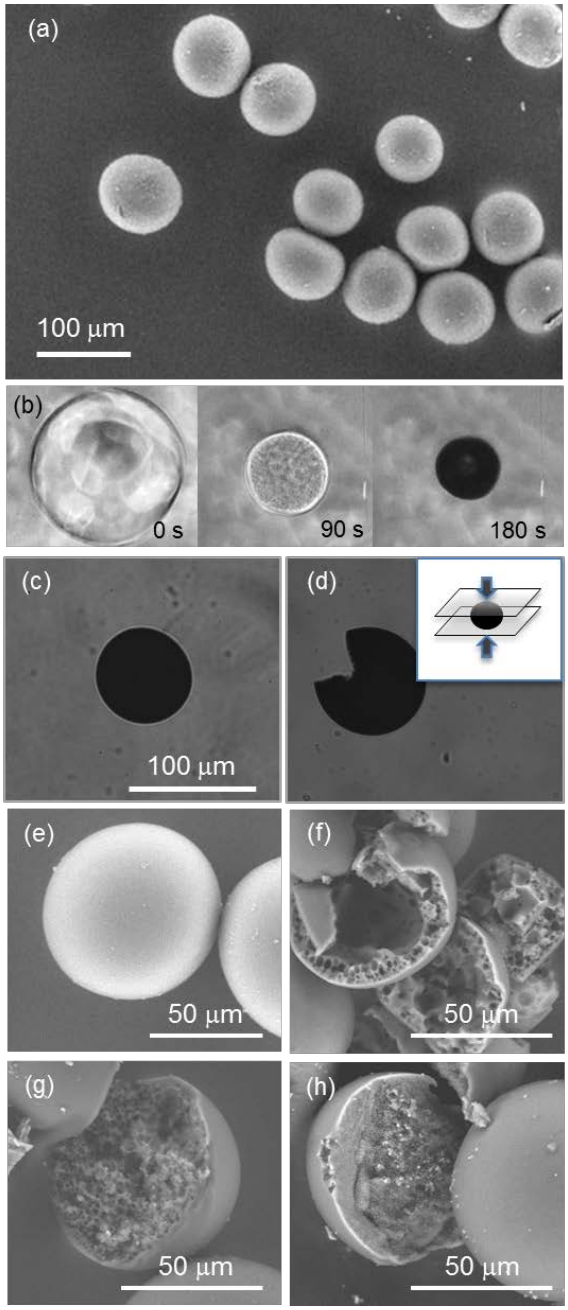

Figure 7. Optical and SEM images of NaPSS particles prepared by solvent extraction. (a) Precipitated 5 wt % NaPSS particles showing smooth particle surface. (b) Time sequence of droplet extraction at intermediate times and optical microscopic images illustrating surface structure. (c,d) NaPSS particle precipitated from a 2.5 wt % aqueous solution before and after compression. (e) SEM image of surface and (f-h) internal structure of microparticles obtained from initial polymer concentrations. (f) $C_{\mathrm{NaPSS,\ t=0}}$ = 2.5 wt %, (g) 5 wt % and (h) 10 wt %.

Generally, the surfaces of solvent-extracted particles are smooth (Fig. 7a) and could suggest a compact object. However, during extraction, transient patterns are occasionally visible on drop surfaces, reminiscent of phase separation or wrinkling, shown in Fig 7b. We found that these surface patterns were not related to the presence of the surfactant, by significantly varying its concentration in the system. From a mechanical perspective, the resulting particles appear to be soft solids (rather than concentrated viscous solutions or glassy materials) and exhibit elasticity following compression. However, when sufficient pressure is exerted, the particles yield and crack (Figs. 7c and d). Figure 7e shows a representative particle prepared from a 2.5 wt % polymer droplet, exhibiting a smooth uniform outer surface. Figure 7f-h illustrates the internal structure of the particles prepared from 2.5 to 10 wt % initial polymer concentrations. Evidently, the particles are internally porous, and the porosity appears to increase gradually towards the center of the particle. For example, particles obtained from polymer droplets at 2.5 wt % exhibit a core-shell structure with a large hollow core and a relatively thick polymer shell. Particles prepared from at 5 and 10 wt % droplets exhibit a denser porous internal structure and, as the initial polymer concentration increases, smaller average pore sizes. This gradient porosity is reminiscent of membrane formation via phase inversion,[23] when a supported polymer dope is immersed into a non-solvent that causes phase separation and then precipitation of the polymer. Upon droplet extraction by selective solvent MEK, the solvent exchange at the drop interface causes drop shrinkage, as water diffuses out, and polymer concentration and viscosity increase and then precipitation within the droplet. Beyond a certain threshold concentration, the polymer ternary solution phase separates and the polymer-rich skin solidifies, as the glass transition of NaPSS is well above room temperature (>130°C, depending on degree of

sulfonation). The porous internal particle structure appears thus to result from the interplay between coarsening of the phase separated structure and hindered solvent removal, constrained by the polymer skin barrier. Droplet extraction kinetics, depicted in Fig. 7b, indicate that the rate of shrinkage during the final stages of extraction decreases with increasing polymer concentration, suggesting an earlier boundary formation for the lowest concentration and thus larger internal porosity, compatible with the observations. Coarsening of the phase-separated structure should proceed with time. Upon increasing initial polymer concentration, however, the final rate of shrinkage decreases and the process becomes quicker overall, suggesting that the polymer precipitates at an earlier stage of phase separation, giving rise to the particle's porous internal structure.

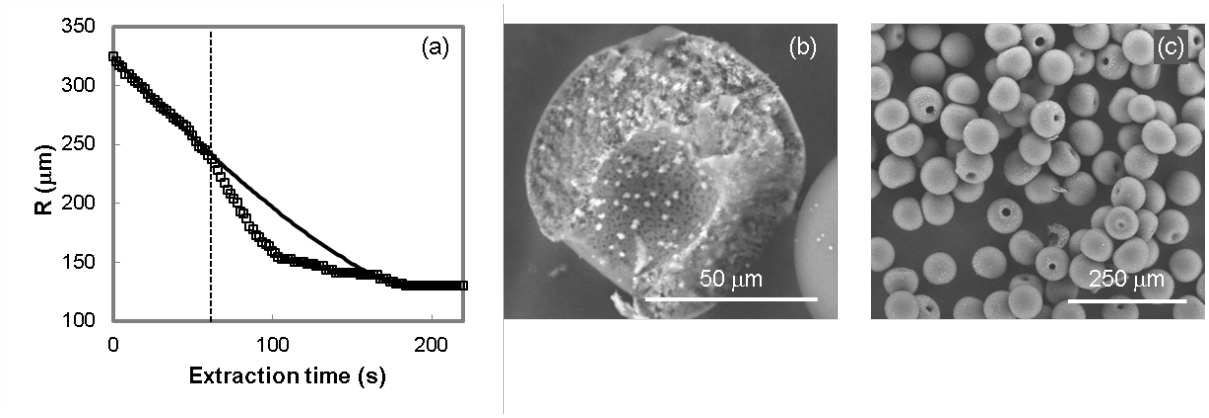

Figure 8 (a) Extraction kinetics of a large droplet (R_0 = 324 μm) of relatively low polymer content ($C_{NaPSS,\ t=0}$ = 2.5 wt %) and the model fitting line. (b,c) SEM images of extracted particles with $C_{NaPSS,\ t=0}$ = 15 wt % and $R_0 \approx 55$ μm, exhibiting a large internal cavity connected to the surface by a single hole.

Unexpectedly, we find that polymer droplets with radius larger than 300 μm exhibit non-monotonic shrinking, even for relatively low polymer concentration, as shown in Fig. 8a.

Similarly to previous observations, the radius decreases nearly linearly within the first 60 s. However, after this initial stage, the extraction rate accelerates up until 100 s and then decreases again, as the size approaches the terminal value. The discontinuity in extraction rate is associated with the formation of a cavity and deformation at surface to accommodate the volume reduction, as happens during spray drying. The droplet size threshold for this cavity formation was found to decrease with increasing polymer content. Figures 8b and 8c show SEM images of the final particle structure extracted from 15 wt % droplets, which comprise a single large cavity connected to the surface, in addition to the porous layer. Evidently, larger particles ($R \geq 300$ μm) and/or higher polymer concentration (≥ 15 wt %) are not suitable for production of defect-free spherical microparticles at these extraction rates.

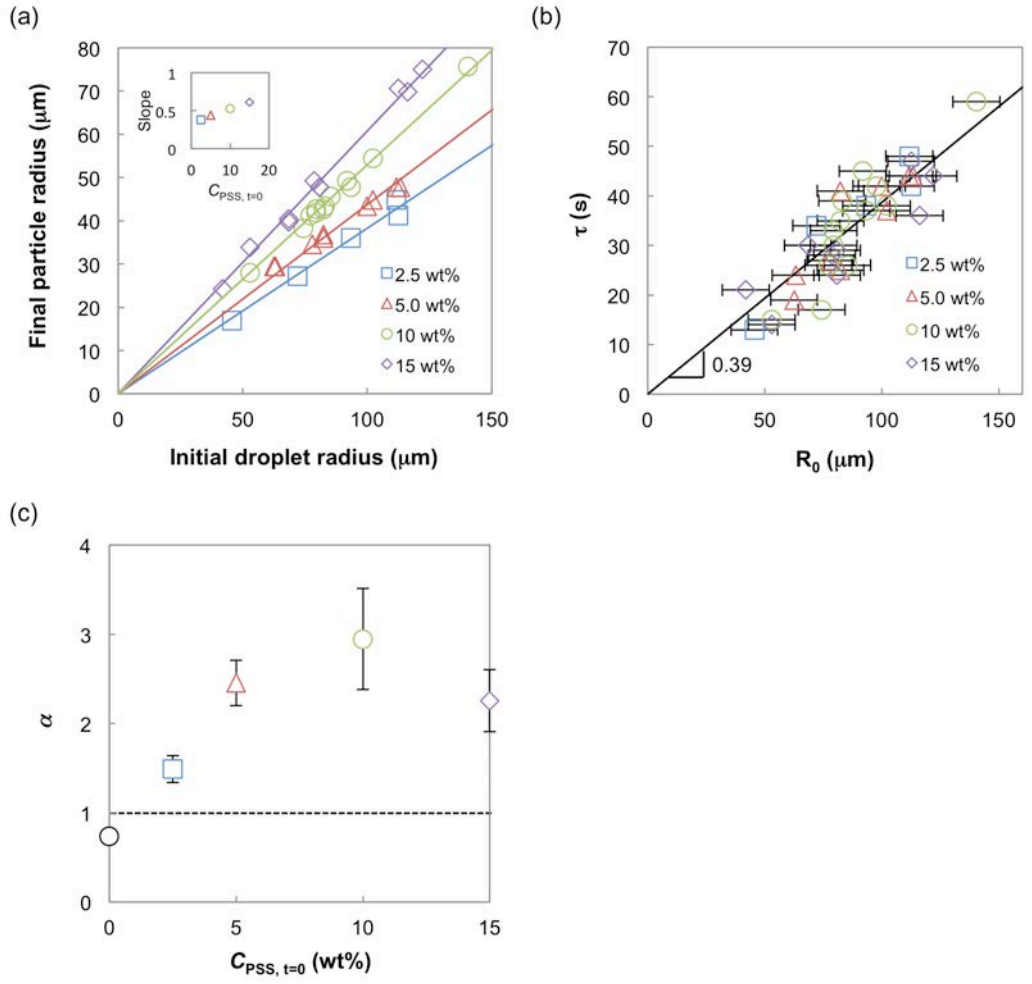

Figure 9 (a) Effect of initial droplet size and polymer concentration on the final particle size; slope is indicated in inset. (b) Effect of initial droplet size and polymer concentration on extraction time. (c) Effect of initial polymer concentration on extraction kinetics.

In Figure 9a we examine the effect of the initial polymer concentration and the initial droplet size on the final particle size. Regardless of the initial polymer concentration, we find a linear relationship between the initial droplet size and the final particle size, albeit with different slopes (indicated in inset). Final particle sizes can thus be estimated from the initial polymer concentration and the initial droplet size, which is beneficial in designing polymer particles. Figure 9b summarizes the dependence of extraction time τ on the initial droplet size, for various initial polymer concentrations. As expected, τ increases with increasing initial droplet size. However, we find that the initial polymer concentration does not affect τ, within the experimental conditions investigated, and the same relation between τ and R_0 applies to all concentrations. The effect of the initial polymer concentration on α is shown in Fig. 9c: it increases with increasing initial polymer concentration, from 0 to 10 wt %, and then slightly decreases at 15 wt %, independently of the initial droplet size within measurement uncertainty. As discussed above, α describes the curvature of the droplet reduction plots during solvent extraction; larger α value means that shrinkage is initially faster and then rapidly slows down in the final stages of extraction.

An *apparent* polymer concentration within droplets and particles can be estimated from the measured volume, based on the initial droplet volume, polymer concentration, and density of each component. The calculation is sensitive to the size measurement and image thresholding, which contributes to large experimental errors. Figure 10a plots the evolution of

apparent C_{NaPSS} with extraction time for several initial droplet sizes and polymer concentrations. Regardless of the initial polymer concentration, the rate increases rapidly beyond a polymer concentration of approximately 13 wt %, that roughly corresponds to the concentration at which the solution viscosity enters the concentrated regime. On the other hand, there is a large variation in the apparent polymer concentration in the particles, ranging from 40 to 80 wt %. The lower initial polymer concentration conditions yield the lower range of final apparent polymer concentration, within 40 to 50 wt %.

Evidently, the particles are internally porous and the calculation assumes particle homogeneity, which yields lower *apparent* C_{NaPSS} for highly porous particles (e.g. those prepared from lower concentration). Particle porosity can be thus estimated assuming complete polymer precipitation, which is reasonable given the large non-solvent excess, from the final particle sizes R_∞. Figure 10b shows the dependence of the calculated pore fraction on the initial polymer concentration. The relatively large uncertainties mirror the distribution of apparent polymer concentration and comprise the propagated uncertainty in droplet volumes. We find that porosity follows approximately the inverse trend of α in Fig. 9c, corroborating our qualitative interpretation of the role of α in setting the relative rates of shrinkage and internal coarsening. In agreement with the SEM data of the internal structure of the particles in Fig. 7, we find that particle porosity decreases with increasing initial polymer concentration, until leveling off beyond 10 wt % PSS.

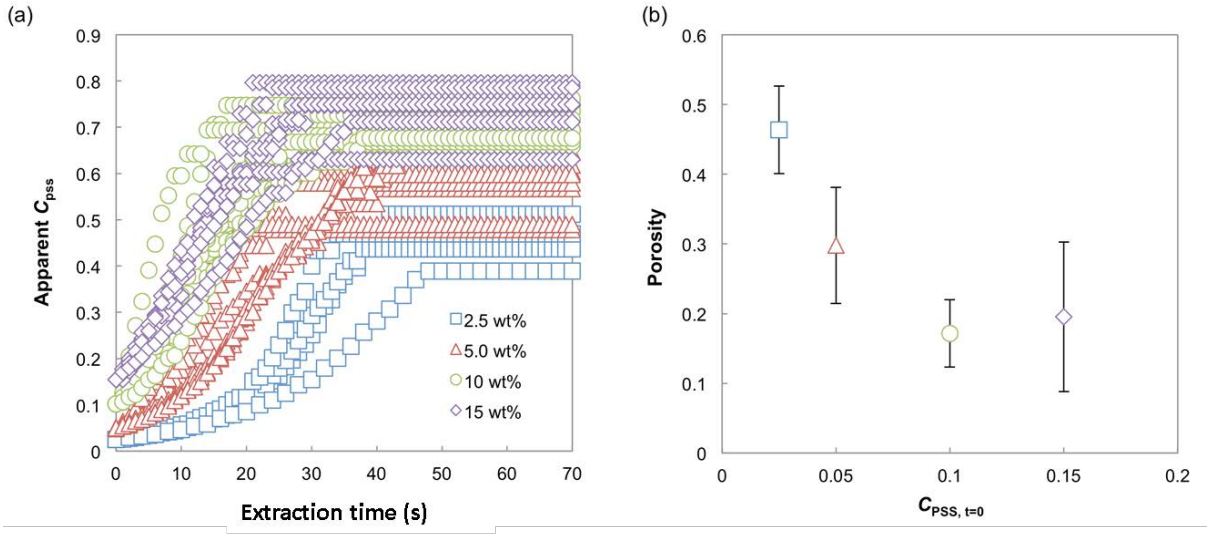

Figure 10 (a) Apparent C_{NaPSS} in the droplets as a function of extraction time, for various initial polymer concentrations (□ 2.5, Δ 5.0, ○ 10, and ◊ 15 wt%) and droplet sizes ($30 \leq R_0 \leq 150$ μm). (b) Calculated microparticles porosity range (%) obtained from droplets with different initial polymer concentration.

Conclusion

We have demonstrated that the coupling of the controlled droplet formation and subsequent selective solvent extraction of a polymer solution provides a promising route for the formation of polymer capsules with internally porous structures in the 10 to 100 μm range. The controlled phase inversion induces droplet shrinkage, skin formation, internal phase separation and coarsening, forming smooth capsules with controlled internal porosity. Polyelectrolyte NaPSS/H_2O plugs were formed in HD and then precipitated in MEK using FPP solvent-resistant microdevices. Microfluidic cascades can readily yield bimodal (or multimodal) particles. We describe the solvent extraction with a simple scaling model and obtain the extraction time τ and a non-Fickian transport parameter, α. We find that τ depends linearly on droplet size R, independently of concentration, within the range studied, and that

final and initial radii are proportional with a constant set by the initial concentration. The internal porosity correlates inversely with α and is set by the initial polymer concentration which, as it increases, alters the internal morphology from a central hollow structure to a gradient porous structures encapsulated by a uniform skin layer. Such internally porous microcapsules could be promising candidates for drug and chemical delivery.

Acknowledgments

We thank Y. Wang and J. Davies for assistance during SEM measurements and microchip fabrication, A.S.H. Aw and L.L. Tan for the bi-disperse droplet experiments, and O.K. Matar for useful discussions on modeling droplet evaporation. We acknowledge the Erasmus Mundus-Beam program for a scholarship for TW and The Royal Academy of Engineering for a Distinguished Visitor Fellowship for JFD.

ASSOCIATED CONTENT

Supporting Information Detailed procedures for microdevice fabrication and additional SEM images of microparticles produced by solvent extraction are provided. This information is available free of charge via the Internet at http://pubs.acs.org/.

AUTHOR INFORMATION

Corresponding Author

*E-mail: j.cabral@imperial.ac.uk

References

1. Polymer Particles, Advances in Polymer Science 175, *Ed. M. Okubo* **2005**.
2. Polymeric Dispersions: Principles and Applications, NATO Asi series C, Ed J. M Asua, Kluwer **1997**
3. K. Masters, Spray Drying Handbook, Halsted Press, New York, N.Y., 1979
4. Vehring, R.; Foss, W. R.; Lechuga-Ballesteros, D. Particle Formation in Spray Drying. *J. Aerosol.Sci.* **2007**, *38*, 728-746.
5. Kumacheva, E.; Garstecki, P. *Microfludic Reactors for Polymer Particles*. *Wiley* **2011**.
6. Shum, H. C.; Abate, A.R.; Lee, D.; Studart, A.R.; Wang, B.G.; Chen, C.H.; Thiele, J.; Shah, R. K.; Krummel, A.; Weitz, D.A. Droplet Microfluidics for Fabrication of Non-Spherical Particles. *Macro. Rapid Comm.* **2010**, *31*,108-118.
7. Xu, S.; Nie, Z.; Seo, M.; Lewis, P.; Kumacheva, E.; Stone, H. A.; Garstecki, P.; Weibel, D. B.; Gitlin, I. Whitesides, G. M. Generation of Monodisperse Particles by Using Microfluidics: Control over Size, Shape, and Composition. *Angew. Chem. Int. Ed.* **2005**, *44*, 724-728.
8. Dendukuri, D.; Pregibon, D.C.; Collins, J.; Hatton, T.A.; Doyle, P.S. Continuous-flow Lithography for High-throughput Microparticle Synthesis. *Nat Mater.* **2006**, *5,* 365-369.
9. Nisisako, T.; Torii, T. Higuchi, T. Novel Microreactors for Functional Polymer Beads. *Chem. Eng. J.* **2004**, *101*, 23-29.
10. Dendukuri, D.; Tsoi, K.; Hatton, T. A.; Doyle, P. S. Controlled Synthesis of Nonspherical Microparticles Using Microfluidics. *Langmuir* **2005**, *21 (6)*, 2113-2116.
11. Xu, Q.; Hashimoto, M.; Dang, T. T.; Hoare, T.; Kohane, D. S.; Whitesides, G. M.; Langer, R.; Anderson, D. G. Preparation of Monodisperse Biodegradable Polymer

Microparticles Using a Microfluidic Flow-Focusing Device for Controlled Drug Delivery. *Small* **2009**, *5*, 1575-1581.

12. Watanabe, T; Kimura, Y.; Ono, T. Microfluidic Fabrication of Monodisperse Polylactide Microcapsules with Tunable Structures through Rapid Precipitation. *Langmuir* **2013**, *29*, 14082–14088.
13. Utada, A. S.; Lorenceau, E.; Link, D. R.; Kaplan, P. D.; Stone, H. A. Weitz, D. A. Monodisperse Double Emulsions Generated from a Microcapillary Device. *Science* **2005**, *308*, 537-541.
14. Quevedo, E.; Steinbacher, J.; McQuade, D.Y. Interfacial Polymerization within a Simplified Microfluidic Device: Capturing Capsules. *J. Am. Chem. Soc.* **2005**, *127*, 10498-10499.
15. Steinbacher, J. L.; Moy, R. W. Y.; Price, K.E.; Cummings, M. A.; Roychowdhury, C.; Buffy, J. J.; Olbricht, W. L.; Haaf, M.; McQuade, D. T. Rapid Self-Assembly of Core-Shell Organosilicon Microcapsules within a Microfluidic Device. *J. Am. Chem. Soc.* **2006**, *128*, 9442-9447
16. Kim, T. K.; Yoon, J. J.; Lee, D. S.; Park, T. G. Gas Foamed Open Porous Biodegradable Polymeric Microspheres. *Biomaterials* **2006**, *27*, 152-159.
17. Lee, J.; Oh, Y. J.; Lee, S. K.; Lee, K. Y. Facile Control of Porous Structures of Polymer Microspheres Using an Osmotic Agent for Pulmonary Delivery. *J. Controlled Release* **2010**, *146*, 61-67.
18. Liu, X.; Jin, X.; Ma, P. X. Nanofibrous Hollow Microspheres Self-assembled from Star-shaped Polymers as Injectable Cell Carriers for Knee Repair. *Nat. Mater.* **2011**, *10*, 398-406.

19. Duncanson, W. J.; Zieringer, M.; Wagner, O.; Wilking, J. N.; Abbaspourad, A.; Haag, R.; Weitz, D. A. Microfluidic Synthesis of Monodisperse Porous Microspheres with Size-tunable Pores. *Soft Matter* **2012**, *8*, 10636-10640.

20. Zhang, H.; Ju, X.-J.; Xie, R.; Cheng, C.-J.; Ren, P.-W.; Chu, L.-Y. A Microfluidic Approach to Fabricate Monodisperse Hollow or Porous Poly(HEMA-MMA) Microspheres Using Single Emulsions as Templates. *J. Colloid Interface Sci.* **2009**, *336*, 235-243.

21. Mikos, A. G.; Sarakinos, G.; Leite, S. M.; Vacanti, J. P.; Langer, R. Laminated Three-dimensional Biodegradable Foams for Use in Tissue Engineering. *Biomaterials* **1993**, *14*, 323-330.

22. Bae, S. E.; Son, J. S.; Park, K.; Han, D. K. Fabrication of Covered Porous PLGA Microspheres Using Hydrogen Peroxide for Controlled Drug Delivery and Regenerative Medicine. *J. Controlled Release* **2009**, *133*, 37-43.

23. Mulder, M. Basic Principles of Membrane Technology, *Kluwer Academic Publishers*, **1996**.

24. Xia, Y.; Whitesides, G. M. Soft Lithography. *Annu. Rev. Mater. Sci.* **1998**, *28,* 153-184.

25. Cabral, J. T.; Hudson, S. D.; Harrison, C.; Douglas, J. F. Frontal Photopolymerization for Microfluidic Applications. *Langmuir* **2004**, *20,* 10020-10029.

26. Harrison, C.; Cabral, J. T.; Stafford, C. M.; Karim, A.; Amis, E. J. A Rapid Prototyping Technique for the Fabrication of Solvent Resistant Structures. *J. Micromech. Micromach.* **2004**, *14*, 153.

27. Wu, T.; Mei, Y.; Cabral, J. T.; Xu, C.; Beers, K. L. A New Synthetic Method for Controlled Polymerization Using a Microfluidic System. *J. Am. Chem. Soc.* **2004**, *126*, 9880-9881.

28. Cygan, Z. T.; Cabral, J. T.; Beers, K. L.; Amis, E. J. Microfluidic Platform for the Generation of Organic-Phase Microreactors. *Langmuir* **2005**, *21*, 3629-3634.

29. Cabral, J. T.; Douglas, J. F. Propagating Waves of Network Formation Induced by Light. *Polymer* **2005**, *46*, 4230-4241.

30. Link, D. R.; Anna, S. L.; Weitz, D. A.; Stone, H. A. Geometrically Mediated Breakup of Drops in Microfluidic Devices. *Phys. Rev. Lett.* **2004**, *92*, 054503.

31. Dobrynin, A. V.; Colby, R. H.; Rubinstein, M. Scaling Theory of Polyelectrolyte Solutions. *Macromolecules* **1996**, *28*, 1859-1871

32. Kaya1, D.; Belyi1, V. A.; Muthukumar, M. Pattern Formation in Drying Droplets of Polyelectrolyte and Salt. *J. Chem. Phys.* **2010**, *133*, 114905.

33. Jullien, M.-C.; Ching, M.-J. T. M.; Cohen, C.; Menetrier, L.; Tabeling, P. Droplet Breakup in Microfluidic T-junctions at Small Capillary Numbers. *Phys. Fluids* **2009**, 21, 072001.

34. Leshansky, A. M.; Pismen, L. M. Breakup of Drops in a Microfluidic T Junction. *Phys. Fluids* **2009**, 21, 023303.

35. Readey, D. W.; Cooper Jr, A. R. Molecular Diffusion with a Moving Boundary and Spherical Symmetry. *Chem. Eng. Sci*. **1966**, *21*, 917-922.

36. Parker, A.; Vigouroux, F.; Reed, W. F. Dissolution Kinetics of Polymer Powders. *AIChE J.* **2000**, *46*, 1290-1299.

37. Cable, M.; Frade, J. R. The Diffusion-controlled Dissolution of Spheres. *J. Mater. Sci.* **1987**, *22*, 1894-1900.

38. Epstein, P.S., Plesset, M. S. On the Stability of Gas Bubbles in Liquid-Gas Solutions *J. Chem. Phys.* **1950**, 18, 1505-1509.

39. Hixson, A. W., Crowell J. H. Dependence of Reaction Velocity upon Surface Agitation. *Ind. Engr. Chem.* **1931**, *23*, 923-931.

40. Costa, P., Lobo J. M. S., Modeling and Comparison of Dissolution Profiles. *Eur. J. Pharm. Sci.* **2001**, 13, 123-133.

41. Duncan P. B., Needham D. Microdroplet Dissolution into a Second-Phase Solvent using a Microdroplet Technique: Test of the Epstein-Plesset Model for an Aniline-Water System. *Langmuir* **2006**, 22, 4190-4197.

42. Poesio P., Beretta G. P., Thorsen T. Dissolution of a Liquid Microdroplet in a Non-Ideal Liquid-Liquid Mixture far from Thermodynamic Equilibrium. *Phys. Rev. Lett.* **2009**, 103, 064501.